

Article

Integration of Photovoltaic-Based Transformerless High Step-Up Dual-Output–Dual-Input Converter with Low Power Losses for Energy Storage Applications

Belqasem Aljafari ¹, Senthil Kumar Ramu ^{2,*}, Gunapriya Devarajan ³ and Indragandhi Vairavasundaram ⁴

¹ Department of Electrical Engineering, College of Engineering, Najran University, Najran 11001, Saudi Arabia; bhaljafari@nu.edu.sa

² Department of Electrical and Electronics Engineering, Sri Krishna College of Technology (Autonomous), Coimbatore 641042, Tamil Nadu, India

³ Department of Electrical and Electronics Engineering, Sri Eshwar College of Engineering, Coimbatore 641202, Tamil Nadu, India; gunapriyadevarajan@gmail.com

⁴ School of Electrical Engineering, Vellore Institute of Technology, Vellore 632014, Tamil Nadu, India; indragandhi.v@vit.ac.in

* Correspondence: senthilme90@gmail.com

Abstract: The synchronous integration of numerous input and output loads is possible with multi-input (MI) and multi-output (MO) DC–DC converters. In this paper, the non-isolated DC–DC converter described, which has a high step-up capability and multiple ports for outputs and inputs for energy storage system (ESS) applications. The voltage level of the converter is changeable. The capacity to provide the large voltage increases with a low duty cycle portion, the ease with which each duty cycle can be controlled, and minimal power losses are all advantages of the proposed design. The proposed system offers advantages for applications requiring energy storage. In the continuous conduction mode (CCM), the operation principles, steady-state evaluation, and extracting of the voltage and current coefficients are performed. The supply sources can be inserted or withdrawn without causing a cross-regulation issue in the proposed converter. Ultimately, the functionality of the proposed structure is examined using simulation and the laboratory prototype that has been implemented. The proposed converter achieved 94.3% efficiency at maximum power. In addition, the proposed converter attained minimum losses with a difference of 28.5 W when compared to a conventional converter.

Keywords: multi-input multi-output; step-up converter; energy storage; DC–DC converter



Citation: Aljafari, B.; Ramu, S.K.; Devarajan, G.; Vairavasundaram, I. Integration of Photovoltaic-Based Transformerless High Step-Up Dual-Output–Dual-Input Converter with Low Power Losses for Energy Storage Applications. *Energies* **2022**, *15*, 5559. <https://doi.org/10.3390/en15155559>

Academic Editor: Nicu Bizon

Received: 8 July 2022

Accepted: 28 July 2022

Published: 31 July 2022

Publisher's Note: MDPI stays neutral with regard to jurisdictional claims in published maps and institutional affiliations.



Copyright: © 2022 by the authors. Licensee MDPI, Basel, Switzerland. This article is an open access article distributed under the terms and conditions of the Creative Commons Attribution (CC BY) license (<https://creativecommons.org/licenses/by/4.0/>).

1. Introduction

Due to the rapid development of power electronic technology, the ESS dependent on batteries or ultracapacitors has been widely employed in various scenarios, such as photovoltaic and wind energy systems, smart grids, electric vehicles, urban rail transportation systems, etc. [1]. The renewable energy (RE) sources are frequently combined with other clean energy sources. The energy source is varied by using numerous inputs in order to boost dependability, and the use of RE sources have DC voltage outputs, and each source has its unique voltage and current features. MI converters are used to decrease the quantity of converters needed to transform the voltage [2,3]. However, MO converters are required to give the necessary power to loads operating at various voltages. A multi-input–multi-output converter (MIMO) is created by a cascading connection of single-input–multi-output (SIMO) and multi-input–single-output (MISO) converters [4]. The MIMO converter provides benefits over multiple individual converters, such as fewer circuit components and conversion phases that will lead toward a more compact design and a cheaper price. In some circumstances, it could be necessary to integrate various renewable sources with varying power levels, such as photovoltaic (PV) panels, fuel cells,

batteries, and ultracapacitors, in order to provide a single load [5]. Therefore, it is important to combine the various energy sources as efficiently as feasible. A MIMO can resolve this problem by combining the advantages of each source into a single converter to provide a controlled DC output and energy storage, or it can provide the AC load after passing through a DC–AC inverter, as shown in Figure 1.

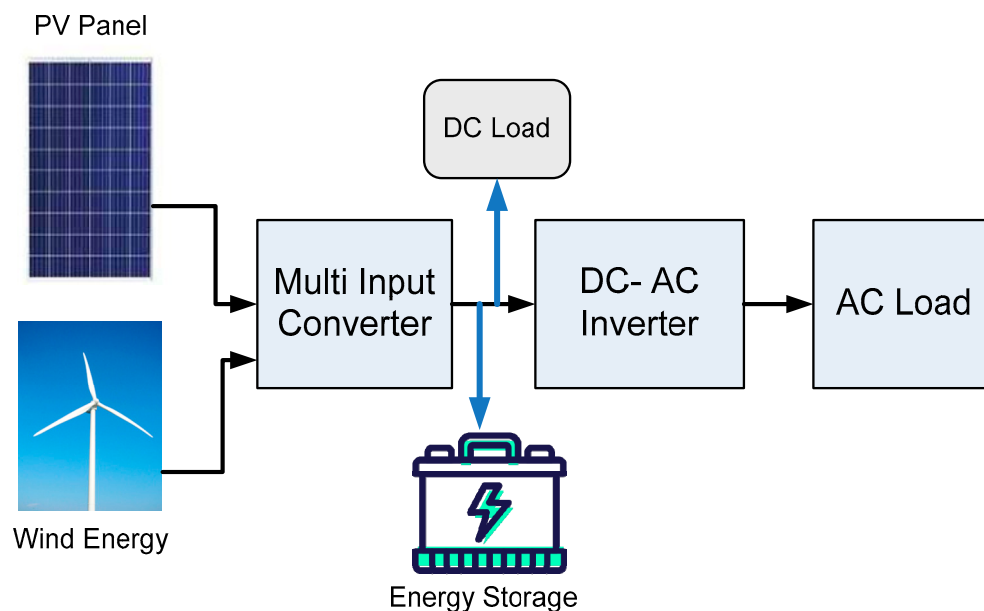


Figure 1. Block diagram of MIMO converter in energy storage.

MIMO converter offers various merits, when compared to single-input–single-output (SISO), SIMO, and MISO converters. A MIMO converter enables customers to employ them in numerous sorts of loads by enabling input from several sources. These converters often assist in combining several sources that produce DC power directly. Due to environmental concerns and the need for stability, research emphasis has recently shifted to micro grids that combine various energy storage devices and renewable energy sources. MIMO converters are essential in such situations for integrating and merging these energy sources to serve the loads when compared to SISO and SIMO converters. The MISO converter is the most often suggested method by researchers to mix various energy sources at various voltage levels [6]. These converters have the drawback of having just one source able to power the load simultaneously. By splitting the current from sources, the MIMO guarantees a seamless transition of power across loads and finally divides the power appropriately when relating to the MISO converter.

MIMOs can be classified as isolated or non-isolated. The isolated-type MIMO uses a transformer with numerous secondary circuits to interact with numerous loads. In this instance, just one of the outputs is highly restricted; the other outputs are connected to additional subordinate windings. In non-isolated MIMOs, there is no electrolytic separation between various ports [7]. Additionally, they are further divided into single and numerous inductors depending on the quantity of the inductive loads. MIMO converters provide the benefits of a lower device count, better power density, and fewer power transmission phases as compared to the traditional DC–DC system design with separate converters. The input cells are typically linked in parallel at the input stage of numerous single inductor MIMO converters, but the output cells may be linked in series or in parallel [8,9]. Due to the common inductor, there is a cross-regulation issue with the output cells that are linked in parallel. Implementing the appropriate control to decrease the reciprocal coupling among output cells coupled in parallel is inherently difficult [10].

The charge sharing method for creating numerous outputs is described in [11]. The authors suggested that even in the CCM, the outputs are load-dependent. A MIMO

converter's setup and its transactional and analytical challenges are addressed in [12]. The functionality of this converter family depends on a time-multiplexing technique [13]. There were a lot of cross-regulation issues, since the outputs of this specific type of MPC are all linked to the same switch node. The dynamic responsiveness of the converters discussed before is typically insufficient in terms of efficiency. A DC–DC converter with resonant MI and MO has been developed [14]. To ensure zero-voltage switching (ZVS) including all power switches during both turn-on and turn-off, the control system must adhere to a certain PWM technique. To address the cross-regulation issue, a model predictive control-based digital control system has been presented [15].

In [16], a unique construction for MIMO DC–DC boost converters is put forth, one that features a high switching frequency without a transformer, a constant current, a high voltage gain without a large duty cycle, and a high voltage gain. A unique non-isolated SEPIC-based multi-input structure is discussed in [17] to address the issues with intermittency of discontinuous power supply. The authors of [18] introduce a new double-input architecture built from a boost and Y-source DC–DC converter [19]. A deadbeat-based solution that incorporates input current and output voltage regulation has been suggested to enhance the performance of regulation [20]. These techniques demand some quite challenging computations. A limitless number of input devices cannot be integrated in a large portion of the previous research work because the time-multiplexing regulation cannot be ignored [21]. Furthermore, the shared inductor and the cross-regulation issue cannot be solved when the outputs are connected with one another. In some circumstances, this limitation exponentially increases the related control complexity. There are various uses, including solar power supply, energy storage, and Internet-of-Things (IoT) devices, despite the non-common ground caused by the series assembly type [22,23]. The design technique is rigorously followed to obtain the controller's optimal performance. In this research, a dsPIC30F4013 controller was used to execute the proposed converter.

A switched capacitor-based MIMO converter with a high voltage gain and an easy control scheme is given in [24]. But the number of components is very high. A boost converter using MIs and MOs has been proposed in [25], and it is appropriate for combining various energy sources in EVs. The inability to use two sources together is a drawback of this arrangement. In [26], a non-isolated MIMO converter with a high gain and no linked inductor was constructed. With this converter, the voltage increase ratio is greater. However, compared to the proposed converter, it has less voltage gain. The MI step-up converter is reported in [27] for integrating several energy sources. However, the voltage gain of this converter is less than the proposed converter. Hence in this paper, non-isolated structure, high voltage gain, minimum number of components are considered to design the proposed converter.

This paper focuses on analyzing and proposing a new MIMO boost converter with high efficiency and constant input and output currents. There is no requirement for time-multiplexing, and the accompanying control technique is fairly simple. In addition, adjustable additions and deletions of inputs and outputs are possible without altering the control strategy. The proposed converter enables the two inputs to feed the load simultaneously with a continuous input current. As a function, this arrangement is very generic for expansion, has uncomplicated control, is highly flexible, and has no cross-regulation issue.

The structure of this paper is as follows: The operation of the proposed converter is provided in Section 2. The steps in the proposed converter's design are described in Section 3. The simulation and experimental results of the proposed converter are discussed in Section 4. A comparison of the results obtained to previously released works is shown in Section 5. The paper's conclusion is the focus of Section 6.

2. Operation of the Proposed Converter

In its most basic form, an MI converter is a circuit layout that incorporates several input voltage sources with various voltage levels and delivers an output DC load. If a

DC–DC converter is synthesized using a pulsing voltage source, or a pulsating current source relies on the characteristics of circuits and systems [28], these modules must be linked in parallel to provide the load in the event of pulsing current sources, such as boost converters. This paper studies and analyses the converter’s MI and MO configurations, which are depicted in Figure 2.

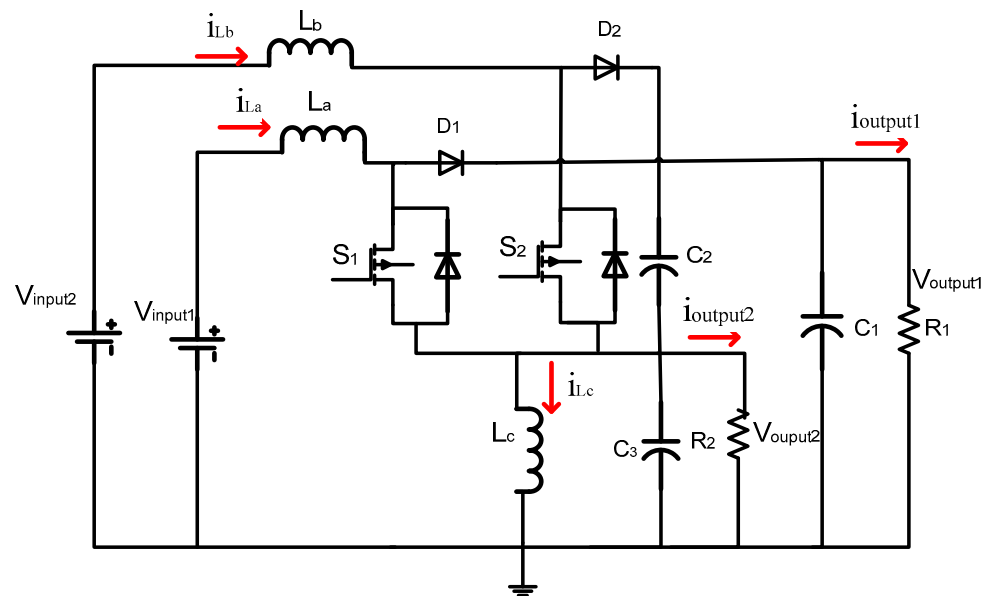


Figure 2. Circuit diagram of proposed converter.

Each of the pulsing current sources is made up of inductors (L_a and L_b), diodes (D_1 and D_2) and power switches (S_1 and S_2). They are each linked to various voltage sources at various voltage levels, notably V_{input1} – V_{input2} . Additionally, regardless of the switching strategy, the capacitors C_1 and C_3 and the inductor L_c are to guarantee the output current’s continuance. The proposed converter’s working principal is explained below, with discussions of theoretical voltage and current studies of each CCM and discontinuous conduction mode (DCM).

2.1. Mode 1 Operation

The schematic diagram of Mode 1 is represented in Figure 3. In Mode 1, switch S_1 conducts, while switch S_2 remains non-conducting at the beginning of this time period. The corresponding time period is represented as T_{on} . Since the inductor L_a ’s current rises proportionately as a result of being closely linked to the first voltage input (V_{input1}), the amount of energy that can be stored in L_a also grows. Diode D_1 is reverse-biased. As a result, the output load’s currents are provided by the inductors L_b and L_c via the capacitors C_1 and C_3 . To do this, there is a steady reduction in the stored energy of C_1 , C_3 , L_b , and L_c .

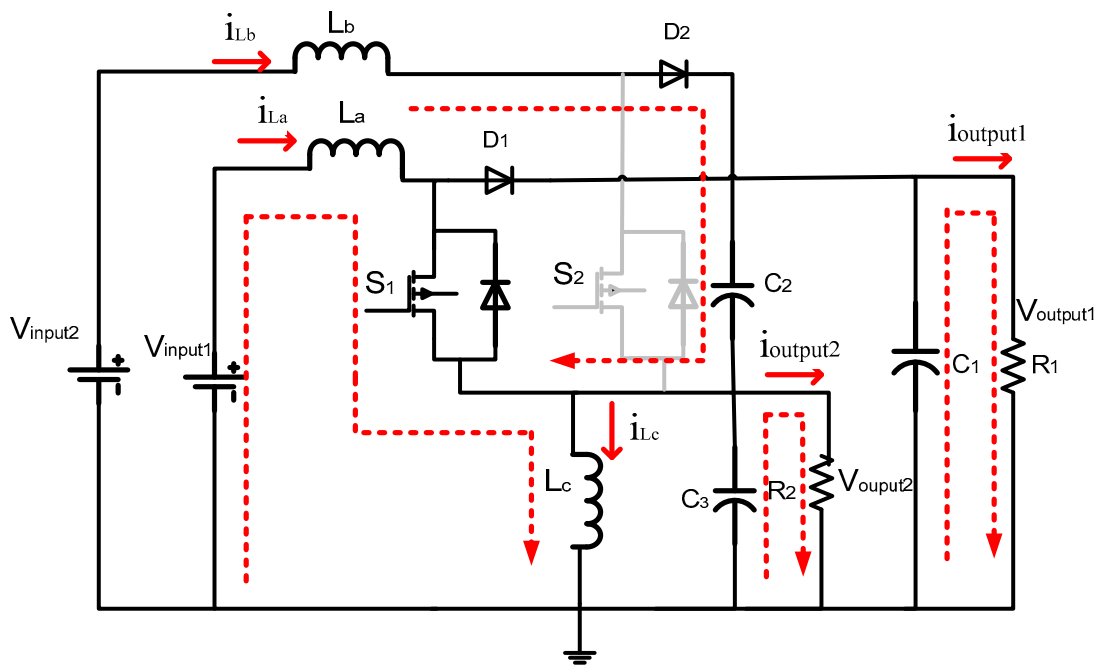


Figure 3. Mode 1 operation (— Current flow direction).

2.2. Mode 2 Operation

The schematic diagram of Mode 2 is represented in Figure 4. In this state, switch S_1 is turned off, while switch S_2 is active. The period of time is now represented as T_{off} . In this mode, the circuit is supplied by input source V_{input2} , which are both present. Reverse bias is present in diode D_1 . As a result, the capacitors C_1 and C_3 and the inductors L_b and L_c , are linked. L_a 's current is thereafter sharply decreased from its peak level to bottom value as a result of the energy stored in L_a being recycled to inductor L_c and capacitor C_3 . As a consequence, from its lowest value to its highest value, the current passing through L_b and L_c is sharply increased. The capacitors C_1 and C_3 's voltages are increasing. The key waveforms under the CCM condition are displayed in Figure 5.

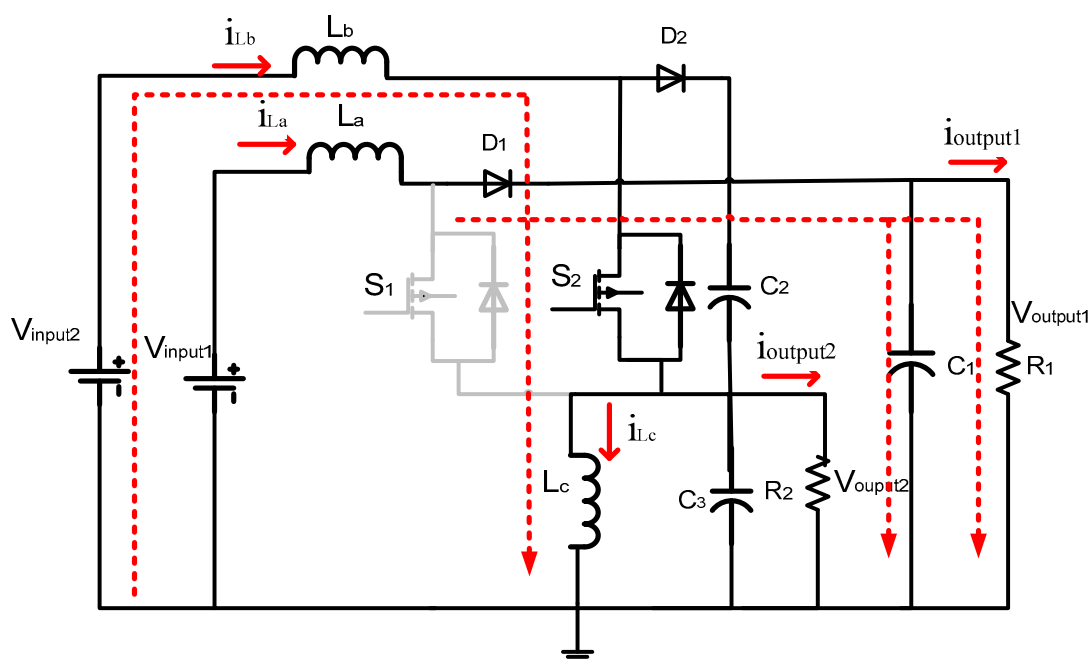


Figure 4. Mode 2 operation (— Current flow direction).

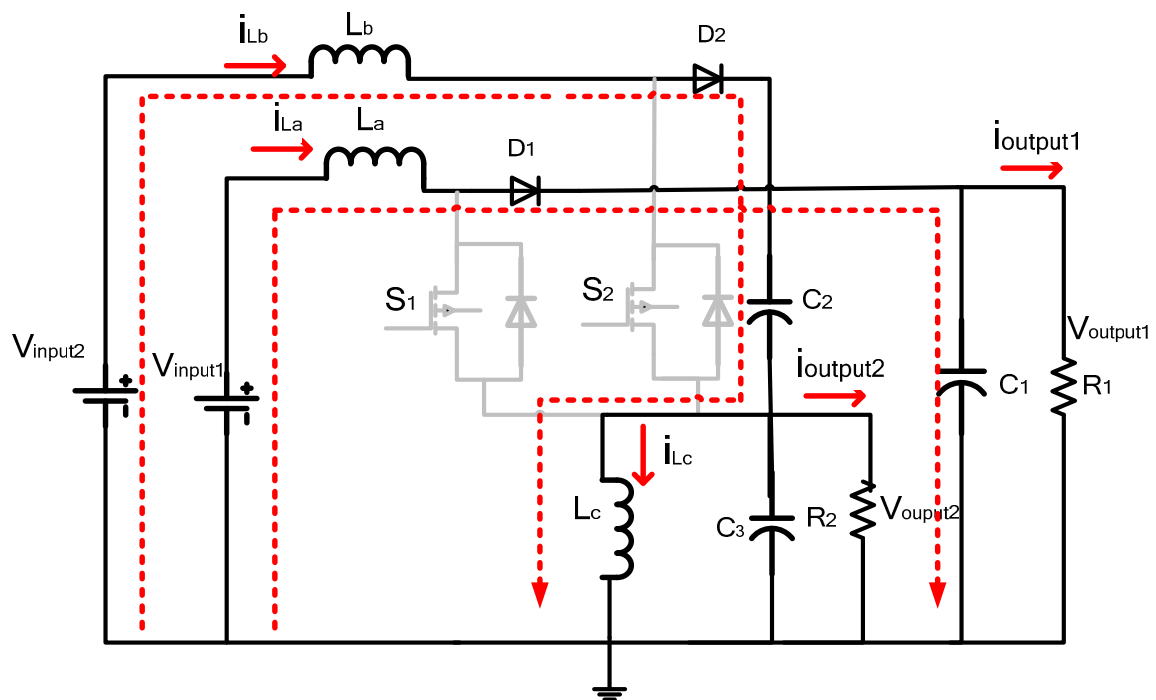


Figure 5. Mode 3 operation (— Current flow direction).

2.3. Mode 3 Operation

The schematic diagram of Mode 3 is represented in Figure 5. In this state, both switches S_1 and S_2 are turned off. The stored energy in L_b is released through D_2 for charging C_2 , and the energy stored in L_a is supplied to R_1 at the same time. Currents going through L_a and L_b are gradually decreased. The key waveforms are displayed in Figure 6.

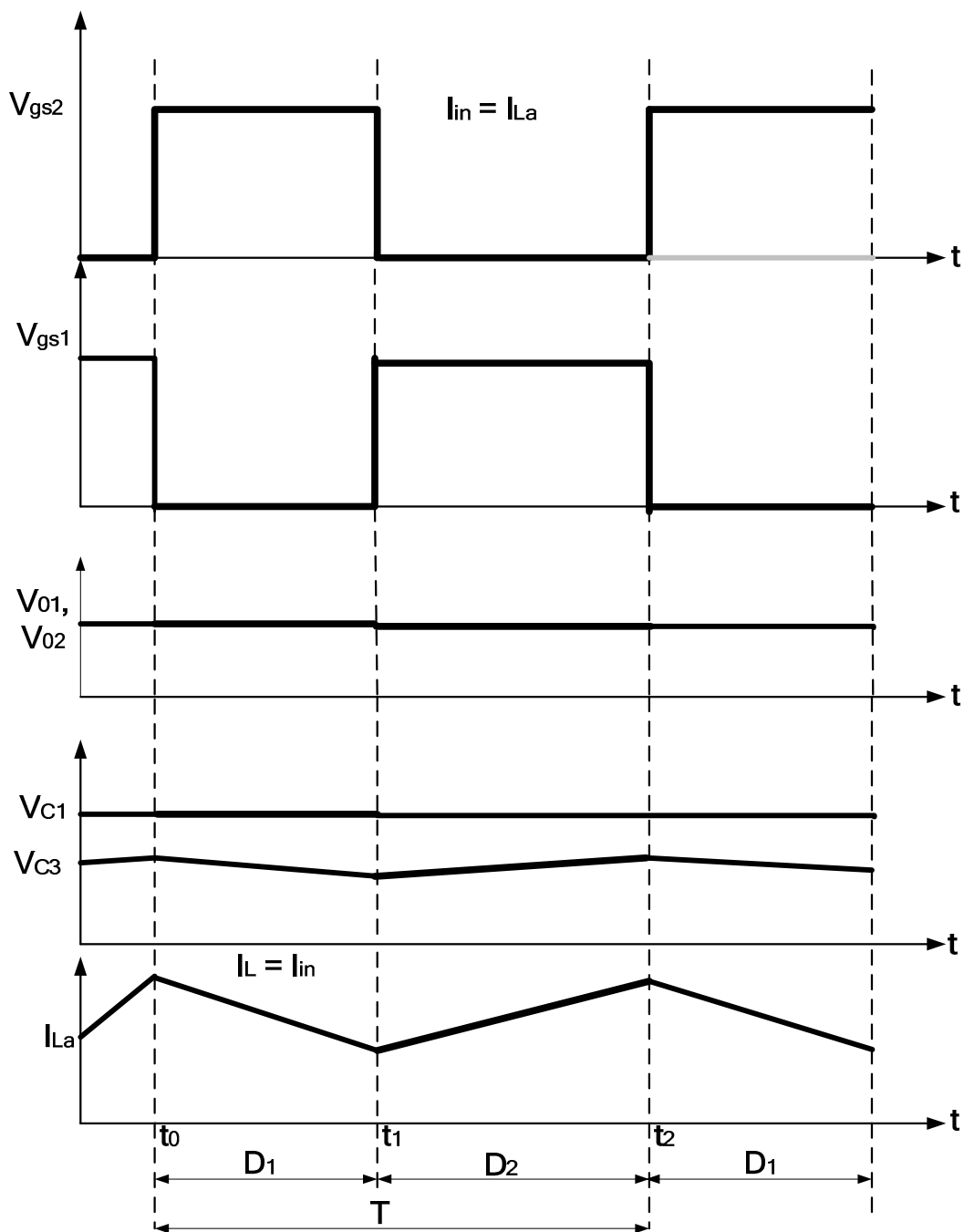


Figure 6. The proposed converter's theoretical operational waveform.

3. The Proposed MIMO Converter's Design Process

The basic control strategy on the input side involves controlling the input sources while employing the matched input cells as controllable sources. The steady-state flow analyses are only computed in the CCM since the converter operation is chosen in CCM. Under the CCM scenario, the optimum voltage gain of the proposed converter is first determined, followed by the average current of the power components. The equipment's current stress predictions are determined in the last phase.

It is possible to regulate the output cells separately. Direct duty cycle control is achieved using the switches S_1 and S_2 of the output voltage source mode (VSM) cell if a controllable output current is needed [29]. Voltage-programmed regulation can be used when a controlled output voltage is necessary. We show the MI and MO types of

the proposed converter here with an experiment, where one output provides a constant current via direct duty cycle control, while the second output delivers constant voltage via voltage-programmed regulation. Here, the MI and MO types of the proposed converter are presented, where the first output offers a fixed current, and the second output delivers a fixed voltage.

3.1. Voltage Gain

The output voltages of the converters are,

$$V_{Output1} = V_{c1} = \frac{V_{input1}}{1 - D_1} = \frac{5}{1 - 0.79} = 23.80 \text{ V} \quad (1)$$

$$V_{Output2} = V_{c3} = \frac{V_{input2}}{1 - D_2} = \frac{12}{1 - 0.67} = 36.36 \text{ V} \quad (2)$$

This configuration's conversion ratio can be written as [30],

$$G_1 = \frac{V_{output1}}{V_{input1}} = \frac{1}{1 - D_1} \quad (3)$$

$$G_2 = \frac{V_{output2}}{V_{input2}} = \frac{1}{1 - D_2} \quad (4)$$

The load current can be represented as,

$$I_0 = \frac{V_{output}}{R} = (1 - D_1)I_{La} + (1 - D_2)I_{Lb} \quad (5)$$

The inductor current I_{Lc} can be written as,

$$I_{Lc} = D_1I_{La} + D_2I_{Lb} \quad (6)$$

3.2. Power Consumed by Each Source

The closed-loop regulation of the output current of all sources, the inductor current I_{La} , is kept constant. A closed-loop control is also used to adjust the output voltage of the second output. The output and input currents of the VSM cell are directly related to one another. As a result, fixed duty cycle regulation can be used to produce a constant current at the first output. Here, we employ a basic duty cycle regulation to retain the steady output current. Considering that the duty cycle D_1 of switch S_1 and the duty cycle D_2 of switch S_2 are equal, the power produced from the input sources through the associated input cell during ideal circumstances can be stated as,

$$P_{input1} = V_{input1}D_1I_{La} \quad (7)$$

$$P_{input2} = V_{input2}D_2I_{Lb} \quad (8)$$

where I_{La} and I_{Lb} are the steady-state inductor current, and P_{input1} and P_{input2} are the power supplied from the input sources V_{input1} and V_{input2} , respectively. The connection shown below can therefore be obtained:

$$\frac{P_{input1}}{P_{input2}} = \frac{V_{input1}}{V_{input2}} \quad (9)$$

According to the calculations provided, every input source's power consumption is related to its associated voltage when the fixed current regulation is used. It is a result of the switches on the respective input cells having the same duty cycle.

It is important to remember that when there are more than two input cells, some of them are regulated to supply a fixed current, while other inputs are directly controlled by

duty cycle regulation. The functionality of this setup will not be impacted if any of these input cells are removed. Power supplied over the first current of input would instantly rise whenever the power supplied through the second cell diminishes. The direct connection between the input and output currents remains constant at the same moment. In this technique, the input voltage providing the second input cell, i.e., V_{input2} , is subjected to a designing restraint to guarantee appropriate operation. Particularly, V_{input2} needs to be lower than the power needed mostly by the output loads.

The necessary power through the loads P_o can be represented as follows:

$$P_o = (1 - D_1)^2 I_{La}^2 R_1 + (1 - D_2)^2 I_{Lb}^2 R_2 \quad (10)$$

where R_1 and R_2 are the respective loads of the two output cells.

3.3. Inductor Selection

The inductor current selection is significant since it is the primary variable in the entire control strategy. The input and output power must comply with the relationship $P_{in,max} > P_o$ in order for the proposed converter to function properly. The selection of inductor and change in inductor current can be represented as,

$$\Delta i_{La} = \frac{1}{L_a} V_{input1} D_1 T \quad (11)$$

$$L_a = \frac{V_{input1} D_1 T}{\Delta I_{La}} = \frac{V_{input1} D_1}{f \Delta I_{La}} = \frac{5 \times 0.79}{25,000 \times 7} = 0.225 \mu\text{H} \quad (12)$$

$$\Delta i_{Lb} = \frac{1}{L_b} V_{input2} D_2 T \quad (13)$$

$$L_b = \frac{V_{input2} D_2 T}{\Delta I_{Lb}} = \frac{V_{input2} D_2}{f \Delta I_{Lb}} = \frac{12 \times 0.67}{25,000 \times 7} = 0.8 \mu\text{H} \quad (14)$$

The choice of the inductor is crucial to guaranteeing a constant source current for the output cells. The proposed arrangement operates in its worst possible condition when there is just a single source of power going to the output cells, and the switches for the two output cells are continuously off. The source with the fixed input cell is the source that consistently supplies power for the proposed control mechanism.

3.4. Capacitor Selection

The output voltage of the VSM unit should be constant in order to preserve the steady-state connection between the input and the current. The choice of the appropriate capacitor is determined by this criterion. The voltage drop of C_1 can be written as,

$$\Delta V_{C1} = \frac{I_{La}}{f \times C_1} \quad (15)$$

To guarantee a constant output voltage, the values of C_1 and C_3 must meet the inequality shown below:

$$C_1 = \frac{I_{01}}{f \times \Delta V_c} = \frac{2.4}{25,000 \times 15} = 6.4 \mu\text{F} \quad (16)$$

$$C_3 = \frac{I_{03}}{f \times \Delta V_c} = \frac{1.5}{25,000 \times 15} = 4 \mu\text{F} \quad (17)$$

3.5. Stability Analysis

To achieve system stability, the closed-loop poles of the characteristic polynomial should be within the unit circle [30]. Because it transfers the left half of the S-plane to the inside of the unit circle in the Z-plane it preserves compensator stability. The projected error variables must meet at zero from any non-zero beginning value, since the controller

is primarily designed to check the robustness of the control rule. This validates that the system under consideration is stable with the appropriate pole positions. The transfer function of the proposed converter for $C_3 = 4 \mu\text{F}$ is found as follows,

$$H(s) = \frac{6 \times 10^6 s^2 + 3 \times 10^7 s + 11 \times 10^{12}}{4s^4 + 5200s^3 + 7500s^2 - 4 \times 10^5 s + 750 \times 10^{11}} \quad (18)$$

The converter remains steady even when the value of the capacitor C_1 is increased. The system poles, on the other hand, migrate to the right side of the axis, and their imaginary values are falling. As a result, by lowering the imaginary quantities of the poles, the frequency of the converter's dampening variations will be lowered.

4. Results and Discussion

To assess its performance, the proposed converter was simulated under various circumstances. The proposed system was developed and modeled using MATLAB/Simulink software. The values of the parameters are shown in Table 1. Figure 7 shows the input voltage waveforms of the proposed converter. The matching input voltages 5 V and 12 V are kept at a constant state.

Table 1. Design parameters.

Parameters	Symbol	Value
Input Voltages	V_{input1}	5 V
	V_{input2}	12 V
Output Voltages	$V_{output1}$	24 V
	$V_{Output2}$	36 V
Capacitors	C_1	6.4 μF
	C_2	4 μF
	C_3	4 μF
Inductors	L_a	0.225 μH
	L_b	0.8 μH
	L_c	0.8 μH
Load Resistance	R_1	10 Ω
	R_2	15 Ω
Duty Cycle	D_1	0.79
	D_2	0.67
Switching Frequency	F_s	25,000 Hz

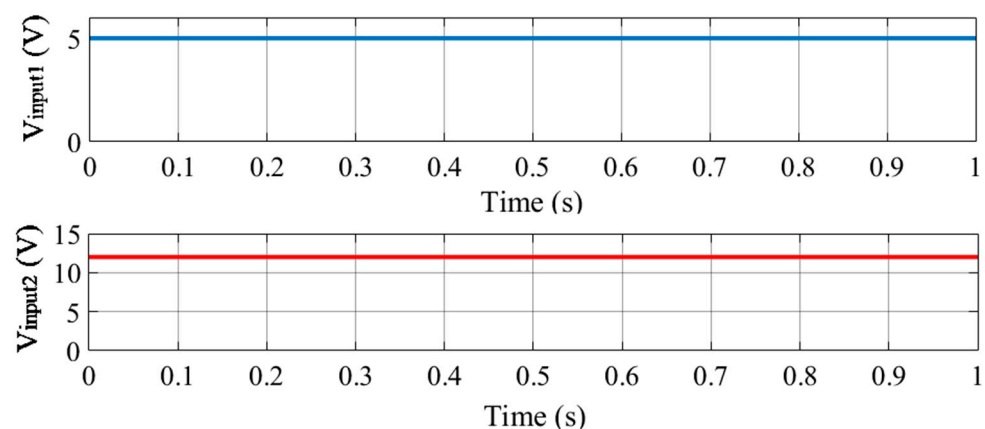


Figure 7. Simulation response of input voltage waveform.

Figure 8 shows the equivalent switching pulse waveforms. The corresponding input voltages 5 V and 12 V are maintained as a steady-state. The corresponding switching pulse waveforms are illustrated in Figure 8. By switching the inductor at a frequency of 25 kHz, the inductor waveform is produced. Figure 9 shows the input inductance currents (I_{La} and I_{Lb}) and the output capacitance ($V_{output2}$). The current in the circuit tries to increase, while the coil stores energy when the switch is turned on, and the input voltages are given to the inductor circuit. The output capacitor provides the load current during this time. The proposed converter has a characteristic that minimizes switching fatigue and capacitive turn-on loss since there is no voltage spike across the switch because the energy stored in the leakage current is released through the diodes in the switch turn-off time. Figure 10 shows the simulation response of the output voltages. The output voltages can produce up to 24 V and 36 V. As a result, it was determined that combining a MIMO converter with a PV system produces 3 to 4 times the amount of input voltages.

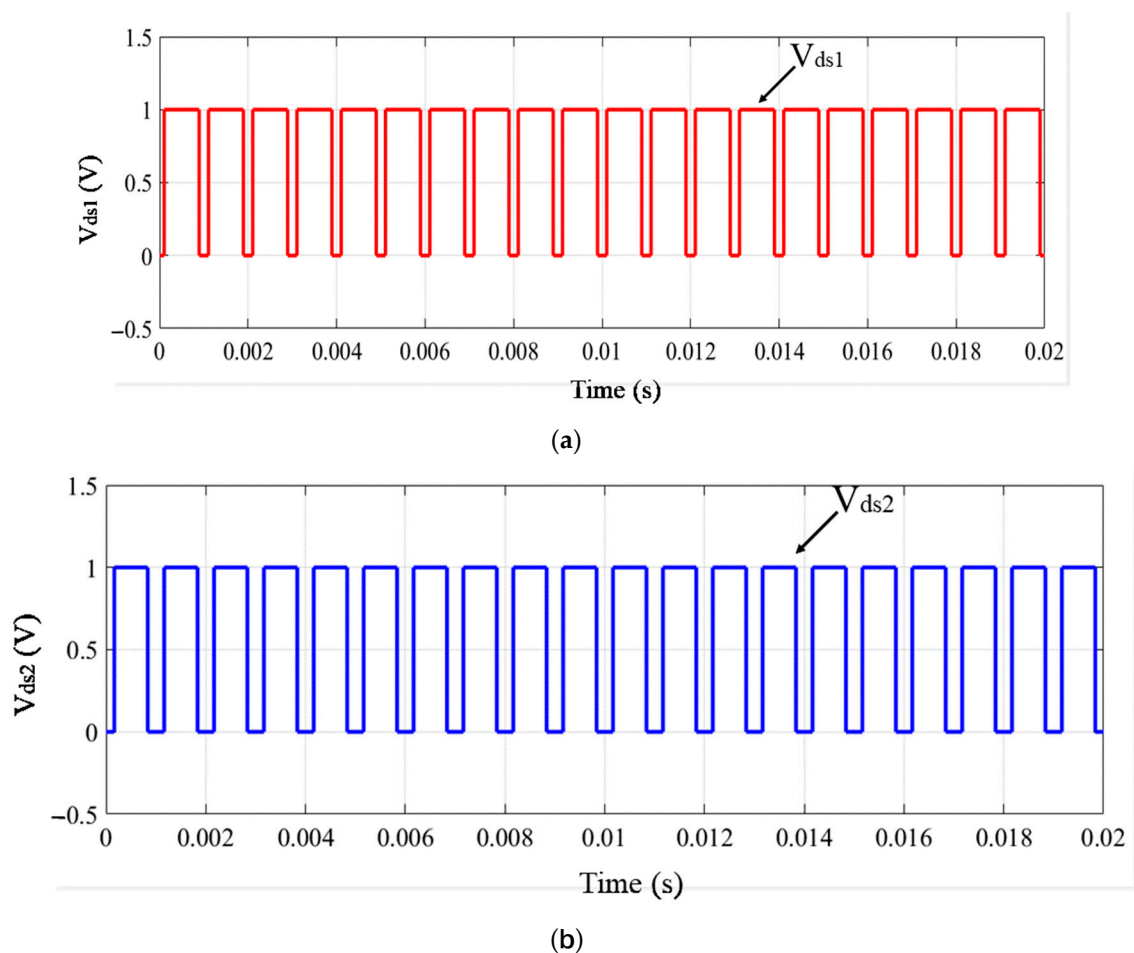


Figure 8. Simulation response of gate pulses (a) V_{ds1} and (b) V_{ds2} .

Experimental Results

To show off the effectiveness of the proposed converter, a lab prototype was designed and is represented in Figure 11. The switching gate pulses are produced using a dsPIC 30F4013 micro controller. The proposed converter was tested under a constant load, step change in load, and variable load change conditions.

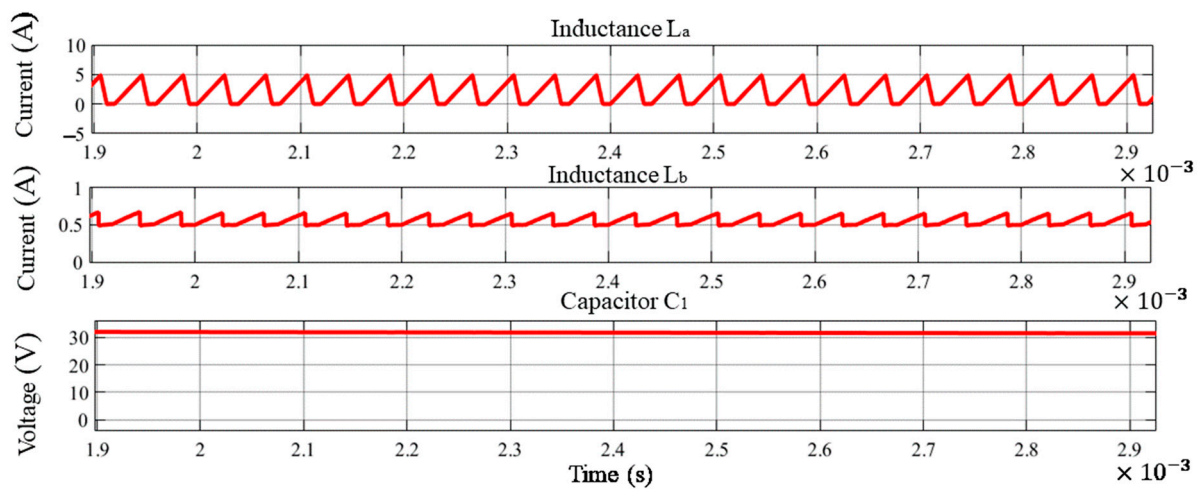


Figure 9. Simulation response of input inductor currents and capacitance voltage.

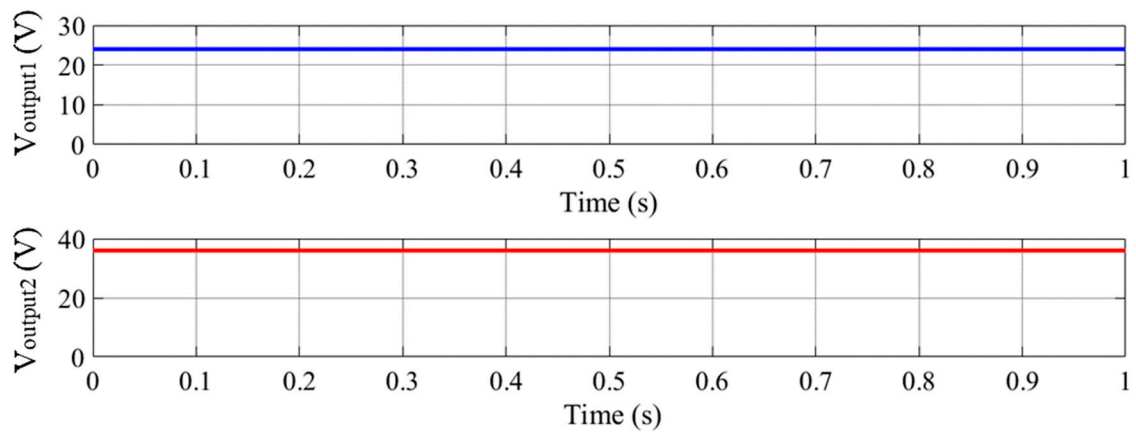


Figure 10. Simulation response of output voltages.



Figure 11. Experimental setup.

When the fixed current control is the supplied input, the appropriate waveform is seen in Figure 12. To assess the converter's ability to balance the voltage, this input voltage (5 V) was recorded during steady-state execution (1 Div. = 5 V). The experimental waveform of input voltage 2 is represented as Figure 13 under a fixed current control state. It demonstrates that the proposed MIMO converter can maintain a steady DC voltage level under CCM while operating with both stable and unstable loads.

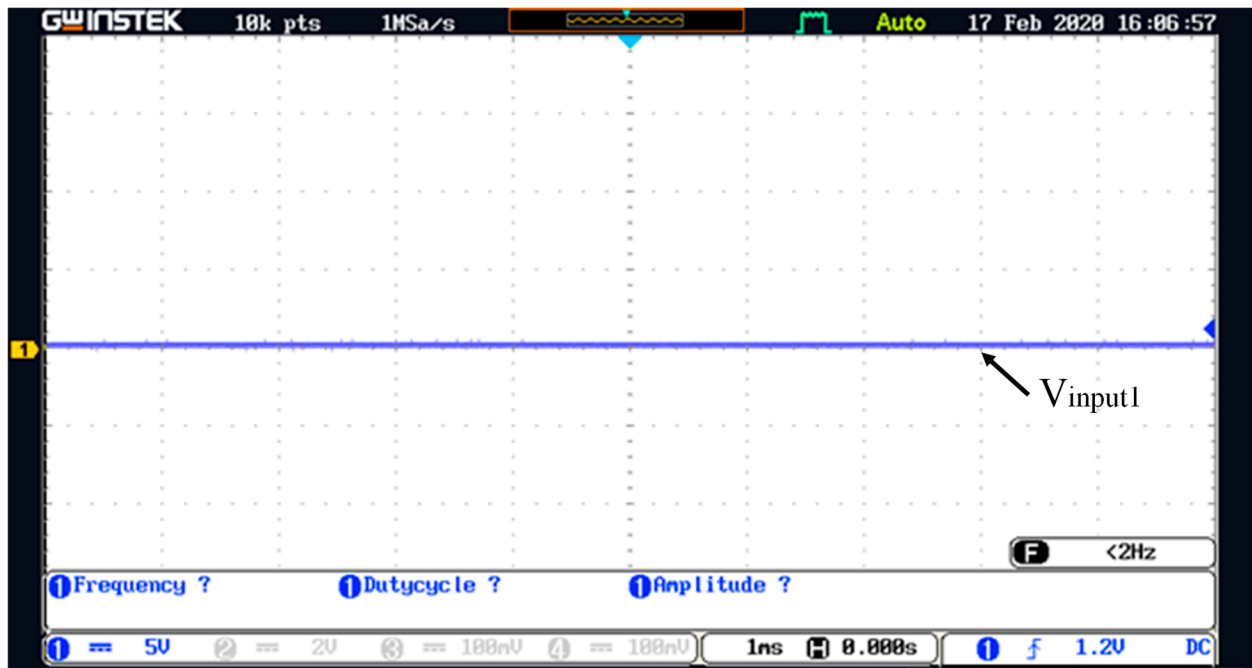


Figure 12. Input voltage 1 waveform.

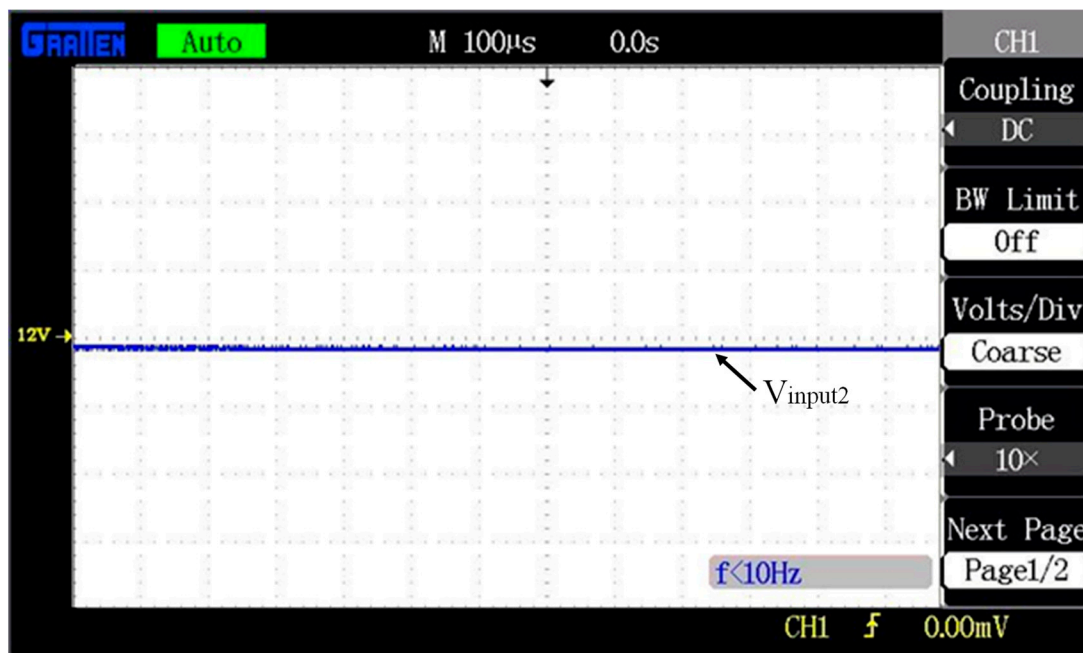


Figure 13. Input voltage 2 waveform.

Figure 14 shows the output voltage 1, the inductance voltage V_{La} , and the drain-to-source voltage of switch 1. The driving signal for the two input units is identical in this scenario since it is produced through closed-loop regulation. The inductive voltage (V_{Lb})

waveform is shown in Figure 15 (1 Div. = 2 V). It displays how the converter can function in two modes when the frequency is pulse-width-modulated. It is important to observe that at the conclusion of each switching cycle, the current flowing through the inductor $L_{a,b}$ becomes continuous. As a result, the proposed converter's operation in the CCM is confirmed. Figure 16 exhibits the output voltage 1 and the drain-to-source voltages of switch 2. Figure 17 depicts the output voltage 2 experiment waveform (1 Div. = 10 V). The proposed converter could deliver many outputs at once, according to the experimental findings. It is clear that duty cycles and switching periods of the two input cells varied. It demonstrates that the input voltage is triple the output voltage.

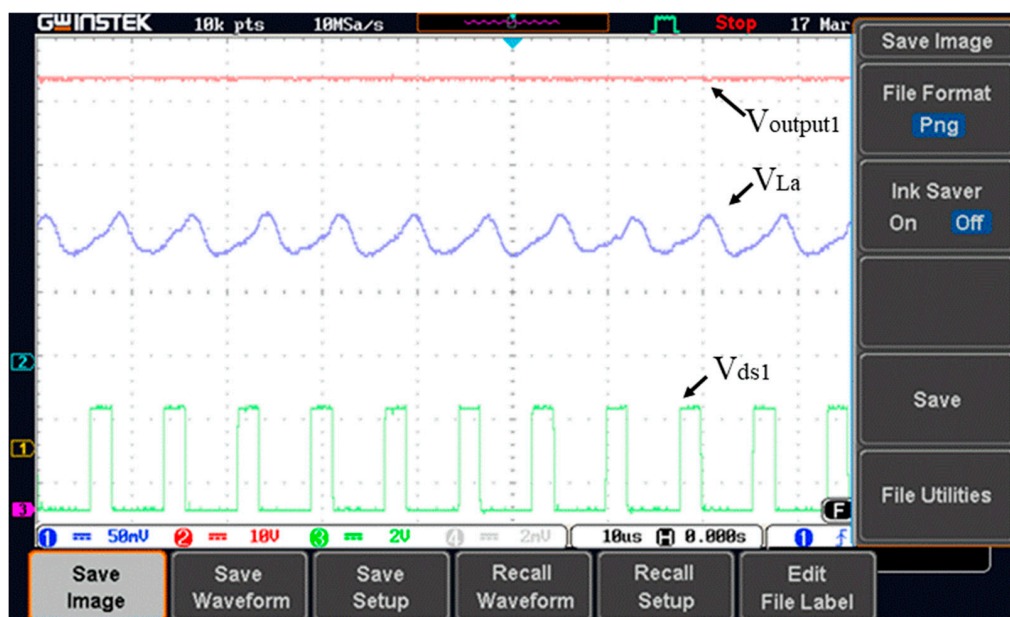


Figure 14. Switching voltage 1, inductor voltage V_{L_a} , and output voltage 1 waveform.



Figure 15. Inductance voltage V_{L_b} waveform.

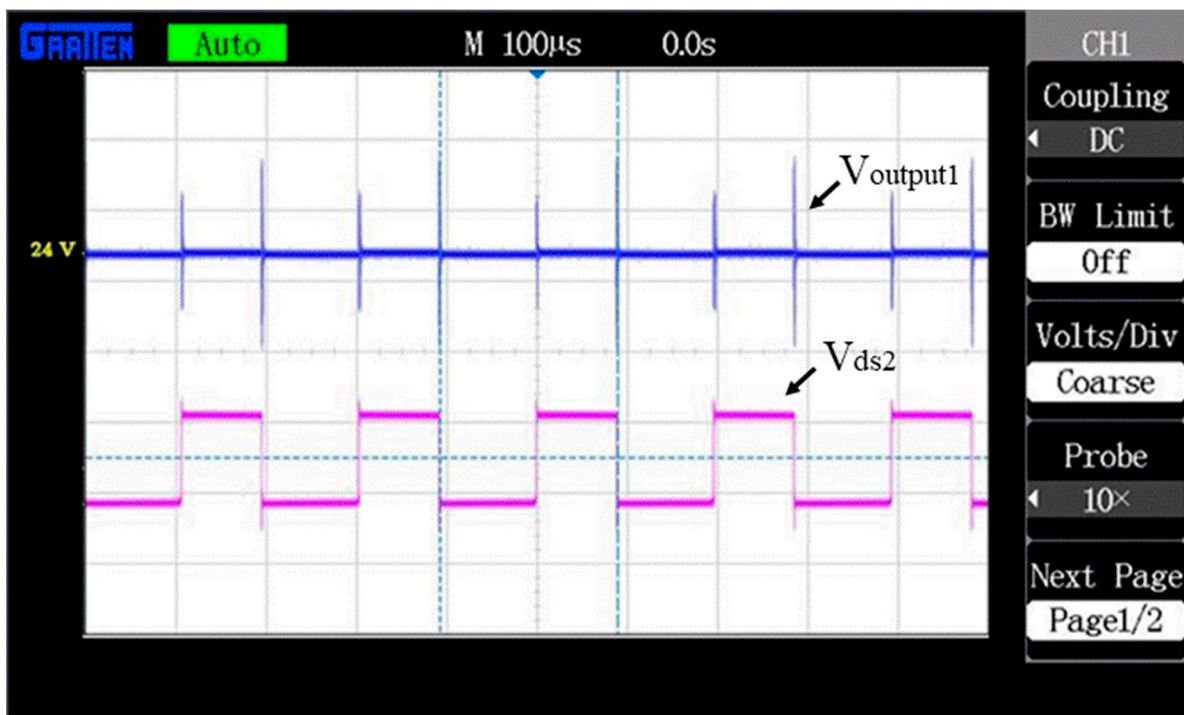


Figure 16. Switching voltage 2 waveform.



Figure 17. Output voltage 2 waveform.

Figure 18 illustrates the relevant functioning waveforms of variable loads under the CCM. The output status is also unchanged as before. We confirm that the two output streams are separate of one another without needing any additional control obtained from the experiments. Therefore, regardless of the quantity of outputs, the control strategy can be the same straightforward constant current regulation. A step voltage command response is shown to demonstrate the proposed multi-objective control. An acceptable overshoot and a disturbance were seen as presented. The proposed converter is integrated into the PV system during fluctuating load under the CCM as shown in Figure 19 (1 Div. = 10 V). This

result implies that the proposed converter can operate with ease in conditions of fluctuating irradiance and load.

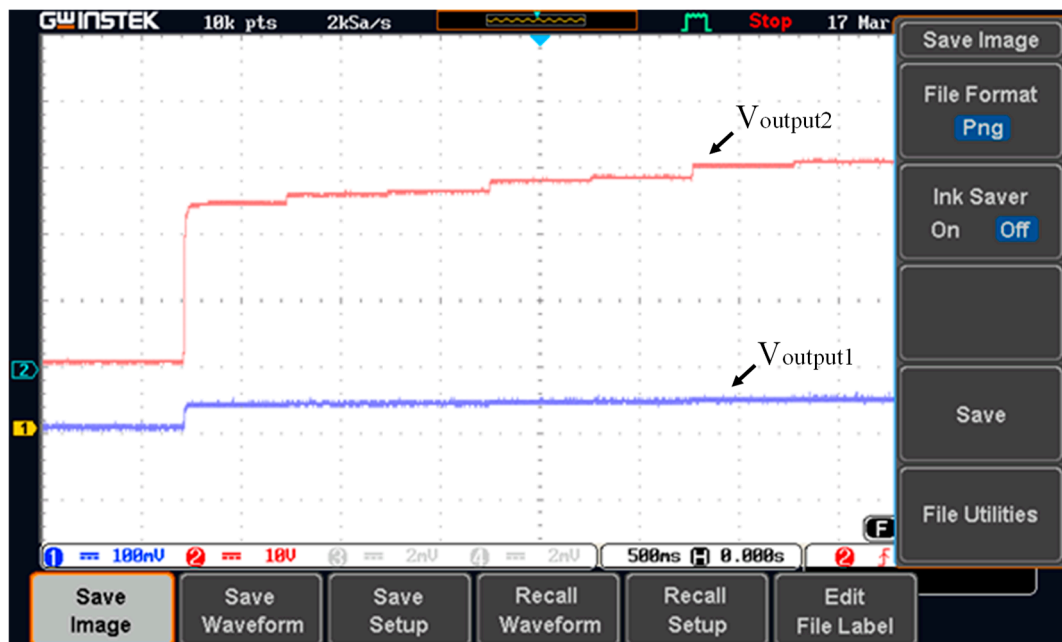


Figure 18. Variable voltages waveform when step change in load.

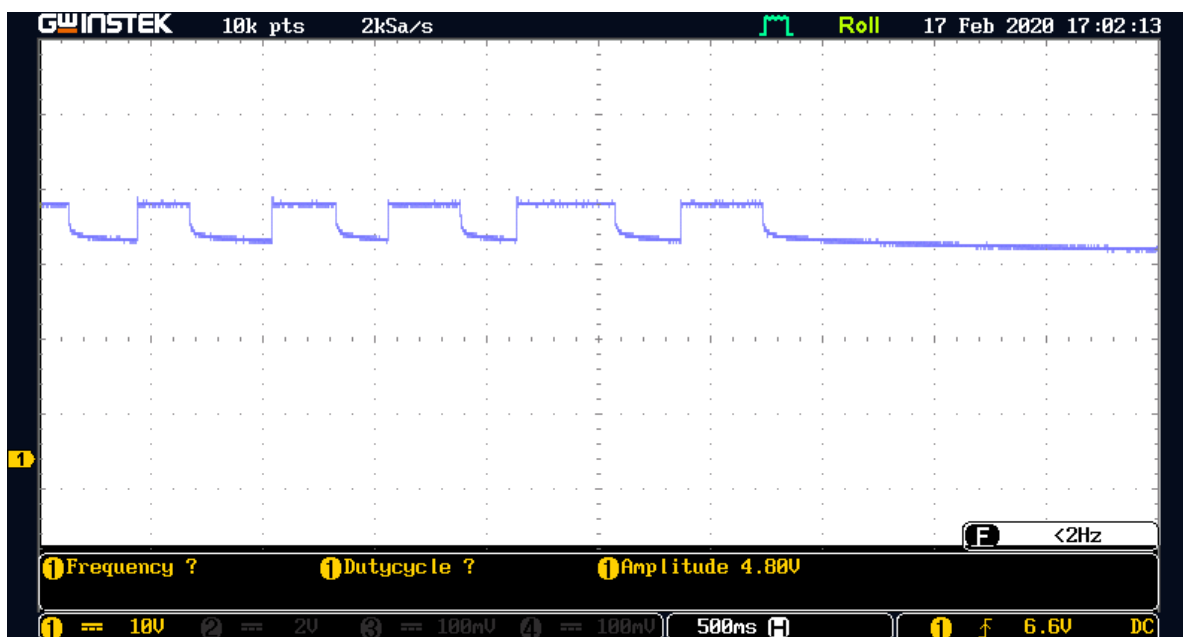


Figure 19. The output voltage ($V_{output2}$) under variable changes in the load conditions.

5. Discussion

A detailed comparative analysis of a proposed converter with existing published converters is provided in Table 2 to further highlight the essential characteristics of the pro-posed converter. These converters are primarily contrasted in terms of converter type, quantity of switches, inputs, outputs, efficiency, and capacity for expansion and inferences. The proposed converter has a fewer number of switches as compared to the previous converters. Since, cross-regulation is not an issue, the appropriate control is simple and very effective. Furthermore, the stability study finds a high power density,

which results in a high extended capacity. Figure 20 compares the proposed converter’s power losses to that of a typical converter, with an anticipated total loss difference of 28.5 W. With conduction losses (S_1 and S_2), inductor core losses, induction winding losses, diode conduction losses, and capacitor losses, the proposed converter has lower losses than the conventional converter. Reduced conduction losses for switches and diodes as a consequence account for most of the efficiency gap between the two converters. The experimental results of the proposed converter’s maximum efficiency under various load conditions are shown in Figure 21. At maximum loading power, the converter efficiency is predicted to be 94.3%.

Table 2. Comparison with existing works.

Ref.	Converter Type	Number of Switches					IV	OV	PD	EC	Stability	Efficiency	Observations
		D	C	S	L	Outputs							
[1]	MIMO high step-up transformerless converter	4	3	4	1	2	30 V, 20 V	21 V, 8 V	Medium	Medium	NR	93.98	Hybrid energy sources integration and MO
[8]	Step-up boost converter with CLD cell	1	5	2	2	2	34 V, 48 V	80 V, 40 V	Medium	Medium	NR	93.4	high voltage gain without maximum value of duty cycle
[12]	Switching boosting action-based MIMO converter	3	5	4	1	2	25 V, 20 V	22 V, 11 V	High	Low	NR	92.1	Improve the power density in various load applications
[16]	Single-inductor MIMO converter	4	3	4	2	1	24 V, 20 V	12 V, 8 V	Medium	Low	NR	89.7	Integration of various loads with minimum number of components
[28]	Single-inductor–multi-input–multi-output DC–DC converter	4	3	4	1	3	18 V, 22 V	12 V, 8 V	Low	Medium	NR	91.5	Integration of multiple loads with fixed current control
Proposed Work	High step-up MIMO Converter with low power losses	2	3	2	3	2	5 V, 12 V	24 V, 36 V	High	High	Reported	94.3	Tarnsformerless MIMO converter with fewer number of switches

D—Diode, C—Capacitors, S—Switch, L—Inductors, IV—Input Voltage, OV—Output voltage, PD—Power Density, EC—Extension capability, and NR—Not Reported.

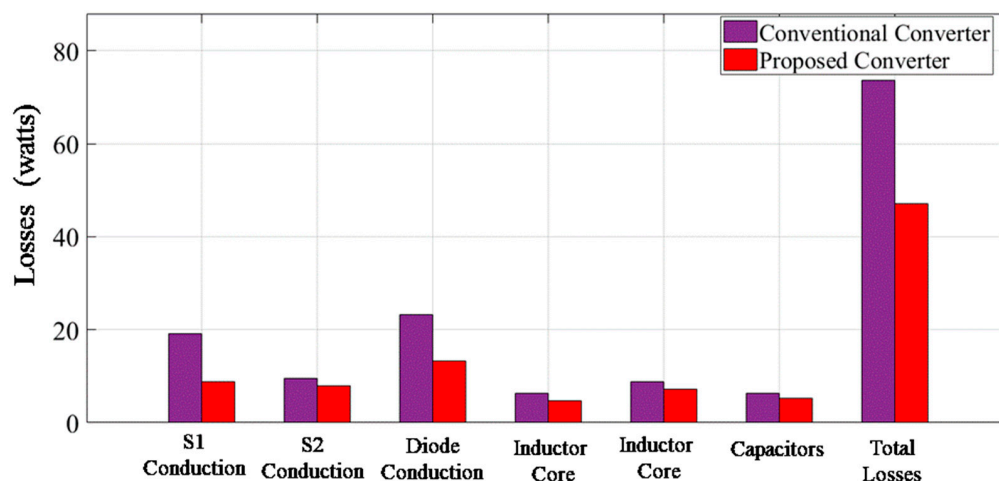


Figure 20. Power loss comparison of proposed converter with traditional converter.

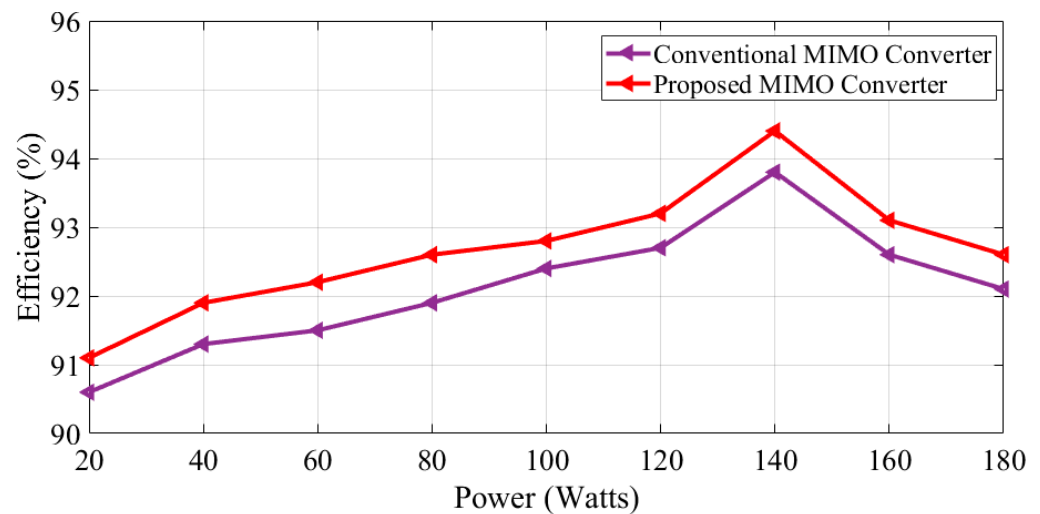


Figure 21. Power versus efficiency graph.

6. Conclusions

This work developed a transformerless and non-isolated rapid step-up MIMO DC–DC power converter with low power losses. The proposed converter is suitable for energy storage applications since it simply has two switches. Because the proposed converter runs in just two operational modes throughout each duty cycle, the converter’s control technique is simple. The performance concepts, theoretical voltage or current assessments, and steady-state analysis have been described. Furthermore, the proposed converter has two voltage gains for the first and second outputs. To ensure that the proposed converter works properly, it was compared to several different topologies. According to the comparative results, the proposed converter has a greater output voltage, fewer components, and minimal power dissipation. To that objective, a simulation and laboratory prototype was built for testing purposes, and experimental findings have been presented.

Author Contributions: Conceptualization, S.K.R.; methodology, S.K.R.; investigation, I.V.; writing—original draft preparation, S.K.R. and I.V.; writing—review and editing, G.D.; resources, B.A.; visualization and administration, S.K.R. and I.V.; funding acquisition, B.A. All authors have read and agreed to the published version of the manuscript.

Funding: This work was funded by the Research Groups Funding program grant code (NU/RG/SERC/11/6).

Institutional Review Board Statement: Not applicable.

Informed Consent Statement: Not applicable.

Data Availability Statement: Not applicable.

Acknowledgments: The authors are thankful to the Deanship of Scientific Research at Najran University for funding this work under the Research Groups funding program grant code (NU/RG/SERC/11/6).

Conflicts of Interest: There are no conflict of interest declared by the authors.

References

1. Saadatizadeh, Z.; Heris, P.C.; Mantooh, H.A. Modular expandable multiinput multioutput (MIMO) high step-up transformerless DC–DC converter. *IEEE Access* **2022**, *10*, 53124–53142. [[CrossRef](#)]
2. Shayeghi, H.; Pourjafar, S.; Hashemzadeh, S.M.; Sedaghati, F. Presenting of the magnetic coupling-based transformer-less high step-up DC–DC converter for Renewable Energy Applications. *Int. Trans. Electr. Energy Syst.* **2022**, *2022*, 3141119. [[CrossRef](#)]
3. Madhana, R.; Mani, G. Power enhancement methods of renewable energy resources using multiport DC–DC converter: A technical review. *Sustain. Comput. Inform. Syst.* **2022**, *35*, 100689. [[CrossRef](#)]
4. Bahrami, H.; Allahyari, H.; Adib, E. An improved wide ZVS soft-switching range PWM bidirectional forward converter for low power applications with simple control circuit. *IET Power Electron.* **2022**, 1–12. [[CrossRef](#)]

5. Appikonda, M.; Dhanalakshmi, K. Small-signal model and control approach for a dual input boost converter with VMC. *Int. J. Electron.* **2021**, *109*, 1035–1058. [\[CrossRef\]](#)
6. Ahmad, F.; Haider, A.A.; Naveed, H.; Mustafa, A.; Ahmad, I. Multiple input multiple output DC to DC converter. In Proceedings of the 2018 5th International Multi-Topic ICT Conference (IMTIC), Jamshoro, Pakistan, 25–27 April 2018.
7. Li, X.L.; Tse, C.K.; Lu, D.D.-C. Synthesis of reconfigurable and scalable single-inductor multiport converters with no cross regulation. *IEEE Trans. Power Electron.* **2022**, *37*, 10889–10902. [\[CrossRef\]](#)
8. Malik, M.Z.; Chen, H.; Nazir, M.S.; Khan, I.A.; Abdalla, A.N.; Ali, A.; Chen, W. A new efficient step-up boost converter with CLD cell for electric vehicle and New Energy Systems. *Energies* **2020**, *13*, 1791. [\[CrossRef\]](#)
9. Shoaie, A.; Abbaszadeh, K.; Allahyari, H. A single-inductor multi-input multi-level high step-up DC-DC converter based on switched-diode-capacitor cells for PV applications. *IEEE J. Emerg. Sel. Top. Ind. Electron.* **2022**. [\[CrossRef\]](#)
10. Dhimish, M.; Schofield, N. Single-Switch Boost-Buck DC-DC converter for industrial fuel cell and photovoltaics applications. *Int. J. Hydrogen Energy* **2022**, *47*, 1241–1255. [\[CrossRef\]](#)
11. Azmoon-Asmarood, S.; Maalandish, M.; Shoghli, I.; Nazemi-Oskuee, S.H.; Hosseini, S.H. A non-isolated high step-up MIMO DC-DC converter for renewable energy applications. *IET Power Electron.* **2022**, *15*, 962–963. [\[CrossRef\]](#)
12. Mishra, S.K.; Nayak, K.K.; Rana, M.S.; Dharmarajan, V. Switched-boost action based Multiport Converter. *IEEE Trans. Ind. Appl.* **2019**, *55*, 964–975. [\[CrossRef\]](#)
13. Saadatizadeh, Z.; Heris, P.C.; Babaei, E.; Sabahi, M. A new nonisolated single-input three-output high voltage gain converter with low voltage stresses on switches and diodes. *IEEE Trans. Ind. Electron.* **2019**, *66*, 4308–4318. [\[CrossRef\]](#)
14. Keyhani, H.; Toliyat, H.A. A ZVS single-inductor multi-input multi-output DC-DC converter with the step up/down capability. In Proceedings of the 2013 IEEE Energy Conversion Congress and Exposition, Denver, CO, USA, 15–19 September 2013. [\[CrossRef\]](#)
15. Gupta, J.; Singh, B. Bridgeless isolated positive output Luo converter based high power factor single stage charging solution for Light Electric Vehicles. *IEEE Trans. Ind. Appl.* **2022**, *58*, 732–741. [\[CrossRef\]](#)
16. Wang, B.; Xian, L.; Kanamarlapudi, V.R.; Tseng, K.J.; Ukil, A.; Gooi, H.B. A digital method of power-sharing and cross-regulation suppression for single-inductor multiple-input multiple-output DC-DC converter. *IEEE Trans. Ind. Electron.* **2017**, *64*, 2836–2847. [\[CrossRef\]](#)
17. Gorji, S.A.; Sahebi, H.G.; Movahed, M.; Ektesabi, M. Multi-input Boost DC-DC converter with continuous input-output current for Renewable Energy Systems. In Proceedings of the 2019 IEEE 4th International Future Energy Electronics Conference (IFEEC), Singapore, 25–28 November 2019.
18. Ramu, S.K.; Paramasivam, S.; Muthusamy, S.; Panchal, H.; Sadasivuni, K.K.; Noorollahi, Y. A novel design of switched boost action based multiport converter using dsPIC controller for Renewable Energy Applications. *Energy Sources Part A Recovery Util. Environ. Eff.* **2021**, *44*, 75–90. [\[CrossRef\]](#)
19. Williams, B.W. DC-to-DC converters with continuous input and output power. *IEEE Trans. Power Electron.* **2019**, *28*, 2307–2316. [\[CrossRef\]](#)
20. Wang, B.; Zhang, X.; Ye, J.; Gooi, H.B. Deadbeat control for a single-inductor multiple-input multiple-output DC-DC converter. *IEEE Trans. Power Electron.* **2019**, *34*, 1914–1924. [\[CrossRef\]](#)
21. Li, Y.; Han, Y. A module-integrated distributed Battery Energy Storage and Management System. *IEEE Trans. Power Electron.* **2016**, *31*, 8260–8270. [\[CrossRef\]](#)
22. Li, X.L.; Dong, Z.; Tse, C.K. Complete family of two-stage single-input multioutput configurations of interconnected power converters. *IEEE Trans. Power Electron.* **2010**, *35*, 3713–3728. [\[CrossRef\]](#)
23. Saadatizadeh, Z.; Chavoshpour Heris, P.; Babaei, E.; Blaabjerg, F.; Cecati, C. Sido coupled inductor-based high voltage conversion ratio DC-DC converter with three operations. *IET Power Electron.* **2021**, *14*, 1735–1752. [\[CrossRef\]](#)
24. Hou, S.; Chen, J.; Sun, T.; Bi, X. Multi-input step-up converters based on the switched-diode-capacitor voltage accumulator. *IEEE Trans. Power Electron.* **2016**, *31*, 381–393. [\[CrossRef\]](#)
25. Nahavandi, A.; Hagh, M.T.; Sharifian, M.B.; Danyali, S. A nonisolated multiinput multioutput DC-DC boost converter for Electric Vehicle Applications. *IEEE Trans. Power Electron.* **2015**, *30*, 1818–1835. [\[CrossRef\]](#)
26. Varesi, K.; Hossein Hosseini, S.; Sabahi, M.; Babaei, E.; Saeidabadi, S.; Vosoughi, N. Design and analysis of a developed multiport high step-up DC-DC converter with reduced device count and normalized peak inverse voltage on the switches/diodes. *IEEE Trans. Power Electron.* **2019**, *34*, 5464–5475. [\[CrossRef\]](#)
27. Deihimi, A.; Seyed Mahmoodieh, M.E.; Iravani, R. A new multi-input step-up DC-DC converter for Hybrid Energy Systems. *Electr. Power Syst. Res.* **2017**, *149*, 111–124. [\[CrossRef\]](#)
28. Li, X.L.; Dong, Z.; Tse, C.K.; Lu, D.D.-C. Single-inductor multi-input multi-output DC-DC converter with high flexibility and simple control. *IEEE Trans. Power Electron.* **2020**, *35*, 13104–13114. [\[CrossRef\]](#)
29. Pourjafar, S.; Sedaghati, F.; Shayeghi, H.; Maalandish, M. High step-up DC-DC converter with coupled inductor suitable for renewable applications. *IET Power Electron.* **2019**, *12*, 92–101. [\[CrossRef\]](#)
30. Samanes, J.; Urtasun, A.; Barrios, E.L.; Lumbreras, D.; Lopez, J.; Gubia, E.; Sanchis, P. Control Design and Stability Analysis of power converters: The MIMO generalized Bode Criterion. *IEEE J. Emerg. Sel. Top. Power Electron.* **2020**, *8*, 1880–1893. [\[CrossRef\]](#)